LAWRENCE
LIVERMORE
NATIONAL
LABORATORY

LLNL-PROC-509414

The Neutron Imaging System Fielded at the National Ignition Facility

D. N. Fittinghoff, D. P. Atkinson, D. E. Bower, O. B. Drury, J. M. Dzenitis, B. Felker, M. Frank, S. N. Liddick, M. J. Moran, G. P. Roberson, P. B. Weiss, G. P. Grim, R. J. Aragonez, T. N. Archuleta, S. H. Batha, D. D. Clark, D. J. Clark, C. R. Danly, R. D. Day, V. E. Fatherley, J. P. Finch, F. P. Garcia, R. A. Gallegos, N. Guler, A. H. Hsu, S. A. Jaramillo, E. N. Loomis, D. Mares, D. D. Martinson, F. E. Merrill, G. L. Morgan, C. Munson, T. J. Murphy, J. A. Oertel, P. J. Polk, D. W. Schmidt, I. L. Tregillis, A. C. Valdez, P. L. Volegov, T. F. Wang, C. H. Wilde, M. D. Wilke, D. C. Wilson, R. A. Buckles, J. R. Cradick, M. I. Kaufman, S. S. Lutz, R. M. Malone, A. Traille

October 28, 2011

Inertial Fusion Sciences and Applications
Bordeaux-Lac, France
September 12, 2011 through September 16, 2011

Disclaimer

THE Neutron Imaging System Fielded at the National Ignition Facility

D. N. Fittinghoff[1a], D. P. Atkinson[1], D. E. Bower[1], O. B Drury[1], J. M. Dzenitis[1], B. Felker[1], M. Frank[1], S. N. Liddick[1], M. J. Moran[1], G. P. Roberson[1], P. B. Weiss[1], G. P. Grim[2], R. J. Aragonez[2], T. N. Archuleta[2], S. H. Batha[2], D. D. Clark[2], D. J. Clark[2], C. R. Danly[2], R. D. Day[2], V. E. Fatherley[2], J. P. Finch[2], F. P. Garcia[2], R. A. Gallegos[2], N. Guler[2], A. H. Hsu[2], S. A. Jaramillo[2], E. N. Loomis[2], D. Mares[2], D. D. Martinson[2], F. E. Merrill[2], G. L. Morgan[2], C. Munson[2], T. J. Murphy[2], J. A. Oertel[2], P. J. Polk[2], D. W. Schmidt[2], I. L. Tregillis[2], A. C. Valdez[2], P. L. Volegov[2], T. F. Wang[2], C. H. Wilde[2], M. D. Wilke[2], D. C. Wilson[2], R. A. Buckles[3], J. R. Cradick[3], M. I. Kaufman[3], S. S. Lutz[3], R. M. Malone[3], A. Traille[3]

[1]Lawrence Livermore National Laboratory, P. O. Box 808, Livermore, CA 94550, USA
[2]Los Alamos National Laboratory, Los Alamos, NM 87545, USA
[3]National Security Technologies, Las Vegas, NV, USA

Abstract. We have fielded a neutron imaging system at the National Ignition Facility to collect images of fusion neutrons produced in the implosion of inertial confinement fusion experiments and scattered neutrons from (n, n') reactions of the source neutrons in the surrounding dense material. A description of the neutron imaging system will be presented, including the pinhole array aperture, the line-of-sight collimation, the scintillator-based detection system and the alignment systems and methods. Discussion of the alignment and resolution of the system will be presented. We will also discuss future improvements to the system hardware. This work was performed for the U.S. Department of Energy, National Nuclear Security Administration and by the National Ignition Campaign partners: Lawrence Livermore National Laboratory (LLNL), University of Rochester -Laboratory for Laser Energetics (LLE), General Atomics (GA), Los Alamos National Laboratory (LANL), and Sandia National Laboratories (SNL). Other contributors include Lawrence Berkeley National Laboratory (LBNL), Massachusetts Institute of Technology (MIT), Atomic Weapons Establishment (AWE), England, and Commissariat à l'Énergie Atomique (CEA), France. Prepared by LLNL under Contract DE-AC52-07NA27344

1 Introduction

A major goal of the National Ignition Campaign (NIC) is to achieve ignition and thermonuclear burn in the laboratory via inertial confinement fusion (ICF) on the National Ignition Facility (NIF) [1] by tuning the parameters of the drive and implosion[2]. Images of thermonuclear neutrons have been used to diagnose capsule performance[3-6], and we have fielded a neutron imaging system (NIS) at

[a] Email:fittinghoff1@llnl.gov

the NIF to collect images of fusion neutrons produced in the implosion of inertial confinement fusion experiments and scattered neutrons from (n, n') reactions of the source neutrons in the surrounding dense material. A description of the neutron imaging system is presented, including the pinhole array aperture, the line-of-sight (LOS) collimation, the scintillator-based detection system and the alignment systems and methods. Discussion of the alignment and resolution of the system will be presented. We will also discuss future improvements to the system hardware.

2 Neutron imaging system description

The NIS is a time-gated, aperture-imaging system similar in concept to an optical pinhole camera, which uses thick aperture to scatter the neutrons and a scintillator to convert the neutrons to light that can be time-gated to provide energy discrimination and detected using CCD detectors.

The NIS is required to measure two images: a primary image with energies from 13-17 MeV and a downscattered image with energies from 10-12 MeV for primary neutron yields from 5 x 10^{15} to 10^{19} neutrons into 4π. To capture the imploded capsule in the images, the field of view of the images needs to be at least 100 μm for the primary image and 150 μm for the downscattered image. The required signal to noise is 22 at the peak of the primary image and ≥10 at the 20% contour. The design described here meets these requirements with the exception of the resolution, which is currently limited to ~22-μm by the location of the aperture array and the quality of the scintillator array as discussed below. While initial prototypes of the NIS design have been discussed [7,8], the design has been modified and an updated description is necessary.

2.1 Line-of-sight and collimation

The neutron imager is mounted on the NIF 90-315 LOS, which is the horizontal LOS at the 315° longitude position. The source is located at the target chamber center (TCC). The LOS starts at TCC and passes through the NIS aperture, which has its front surface 32.5 cm from the source, then through the concrete walls of the Target Bay and Switchyard 1 and enters the NIS Annex where a scintillator converts the neutrons to optical light. The distance from TCC to the scintillator along the LOS is 28 m. To minimize the number of scattered neutrons that can enter the Annex, there are two 38.1-cm Dia., 45.7-cm long collimator stacks made of 304 stainless steel located at the front and back of each of the two concrete walls. The fronts of the four stacks are located 15.239-m, 16.609-m, 23.441-m and 25.183-m from the source along the line of sight. Each stack is tapered in 22.86-cm sections to provide a clear aperture from a 200-μm-diameter source region to a diameter of 198 mm at the 28-m position of the scintillator. A beam stop designed to minimize backscattered neutrons is located at 32.5 m from the source.

2.2 Aperture Design & Alignment

The NIS aperture consists of three mini-penumbral apertures and twenty triangular pinhole apertures, as shown in Figure 1. The apertures are made by scribing six layers of gold that are then sandwiched in tungsten slabs to produce a 1.5-cm wide by 1.5-cm high by 20-cm long aperture body. The mini-penumbral apertures are 273-μm Dia. at the front of the aperture, taper to the center of the pinhole body where they are 300-μm Dia. and taper again to the back of the pinhole where they are 437-μm Dia. The triangular pinholes are 5-μm high at the front of the aperture and have a single taper to 226-μm high at the back. The individual apertures are designed to provide an overlapping field of view at the source that is ~400 μm Dia. Each aperture is also mapped to a corresponding location at the scintillator array such that the images do not overlap.

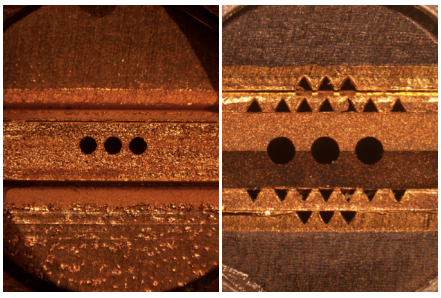

Fig. 1. Front (left) and back (right) of the NIS aperture showing the three mini-penumbral apertures and the twenty triangular pinholes.

Due to the high aspect ratio of the apertures, both the front and back of the aperture array must be aligned to the NIS LOS to high accuracy to maintain the field of view of the system. To simplify the image reconstruction algorithm, our ultimate goal is to align the center mini-penumbral aperture to the axis of the LOS to ±25 μm in the lateral dimensions and ±250 μm in the axial dimension. Due to the difficulty of the alignment, we have initially relaxed these goals to ±50 μm in the lateral dimensions and ±1000 μm in the axial dimension. We set the distance from TCC along the axis of the LOS by using a mechanical pointer attached to the aperture to create a reference position on a reference camera.

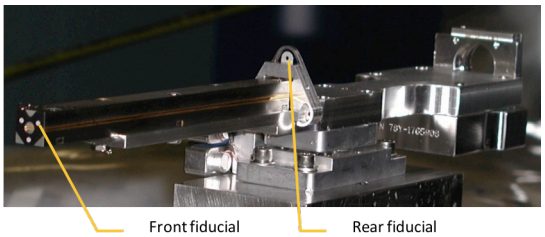

Fig. 2. Alignment fiducials attached to the front and back of the aperture body.

The lateral alignment of the front and back of the aperture array is performed using the opposite port alignment system (OPAS), which is a 11" Celestron Schmidt-Cassegrain telescope that has been modified to image a 100-mm diameter object at TCC and alignment fiducials at the front and rear of the aperture body as shown in Fig. 2. The effective pixel size of the OPAS images is 17.2 μm at TCC. It increases to 18.1 μm at the front face of the NIS aperture, 18.65 μm at the back of the NIS aperture and 95 μm at the scintillator.

For the front fiducials, we use either the mini-penumbral pinholes, which are visible using OPAS, or three 2-mm diameter circles that are bead blasted on a black-anodized aluminum plate. The rear fiducials are three 2-mm diameter holes in thin aluminum plate, which are placed to be visible from the front as well as from the rear to allow viewing by the OPAS. The lateral positions of the fiducials relative to the center mini-penumbral aperture at the front and back of the aperture body were measured using a microscope with an encoded stage and are known to 6-μm accuracy.

While the measurements for the NIS LOS were made using the same precision survey system that was used for NIF construction alignment [9], the OPAS LOS is not identical to it since the OPAS was aimed through TCC to a target at the gimbal point of the diagnostic insertion module (DIM) that is used to hold the NIS aperture. To account for the differences in the lines of sight, we used OPAS to image the targets at the collimators and scintillator that were used to create the NIS LOS, and corrections were made to the expected locations of the fiducials in the OPAS images.

For the actual alignment in the lateral dimension, the front and back fiducials are imaged using OPAS, and then the aperture position is adjusted using picomotor stages to place the fiducials at their expected positions in the OPAS images.

2.3 Scintillator Array and Imaging Detectors

In the NIS Annex, a 160-mm square by 50-mm thick scintillating fiber array made of 250-μm Dia. BCF-99-55 optical fibers made by St. Gobain converts the image to optical light. The emission peak of the scintillating fibers is 435 nm. The array is manufactured by making ribbons of fibers, cutting and stacking them into sub-blocks and then stacking the blocks to create the scintillator array. The light guided to the ends of the array by the fibers is collected using two imagers: one lens-coupled imager [10] and one fiber coupled imager. In both imagers, the image is reduced to match the 36.8-mm square CCD in an SI 1000 camera, which is a 4k x 4k array of 9-μm pixels. The image is also time-gated in an MCPII to provide energy resolution due the time-of-flight of the neutrons. As seen in Fig. 3, the response of the scintillator is not uniform in a flat field image due to variations in the fibers. In addition, there are stacking faults, shears and long range distortions that limit the measured edge spread function of a rolled edge to ~1.2 mm FWHM, which is larger than the expected

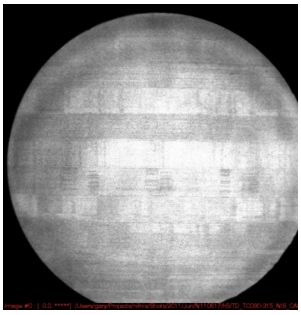
Fig. 3. Flat field image of NIS scintillating-fiber array using the lens-coupled camera. The peak signal is ~10000 CCD counts.

~650-µm point spread function of a 14.1 MeV neutron in the scintillator.

3 Results & future work

We have fielded the neutron imaging system at NIF and have begun obtaining primary and downscattered images of ICF capsule implosions. Neutron images obtained on NIF for shot N110603-002-999, a direct drive capsule, are shown in Fig 4. A reconstruction of the source using a maximum-likelihood method [11] from the center mini-penumbral image is shown in Fig. 5. The magnification is ~98, and the resolution is limited to ~22-µm by a combination of the quality of the scintillator and the current aperture location. Legendre coefficients of fits to the images from the NIS compare well to x-ray images from the same shots. In the future, we expect to improve the resolution by changing the pinhole array and magnification and by developing improved the scintillator arrays. We are also pursuing methods to improve the image reconstruction.

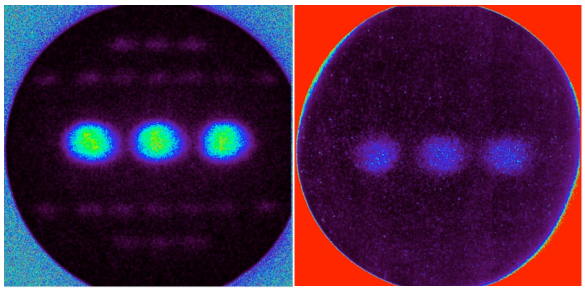

Fig. 4. Neutron images of a direct drive Primary (13-17 MeV) neutron image using lens-coupled arm on the left, and downscattered (10-12 MeV) image on the right. The images are 160-mm square and have been flat-fielded.

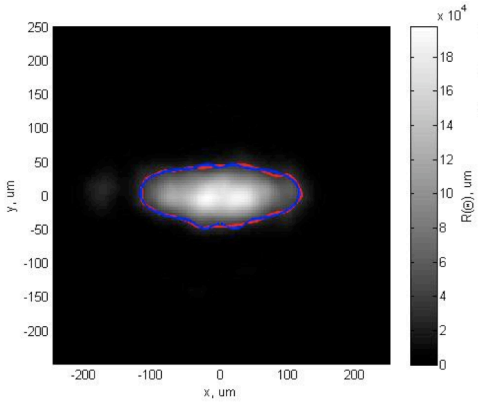

Fig. 5. Primary neutron (13-17 MeV) image reconstructed from center minipenumbral pinhole on left. The red line is the radius of the 17% contour of the image, and the blue line is a Legendre polynomial (P2/P0 = -63%, P3/P0 = -7% and P4/P0 = 36%) fit to that line.

References

1. J. D. Lindl and E. I. Moses, Physics of Plasmas **18** (2011).
2. O. L. Landen, J. Edwards, S. W. Haan, H. F. Robey, J. Milovich, B. K. Spears, . . . D. C. Wilson, Physics of Plasmas **18** (2011).
3. D. Ress, R. A. Lerche, R. J. Ellis, S. M. Lane, and K. A. Nugent, Science **241**, 956 (1988).
4. D. Ress, R. A. Lerche, R. J. Ellis, S. M. Lane, and K. A. Nugent, Review of Scientific Instruments **59**, 1694 (1988).
5. C. R. Christensen, D. C. Wilson, C. W. Barnes, G. P. Grim, G. L. Morgan, M. D. Wilke, . . . C. Stoeckl, Physics Of Plasmas **11**, 2771 (2004).
6. L. Disdier, A. Rouyer, I. Lantuejoul, O. Landoas, J. L. Bourgade, T. C. Sangster, . . . R. A. Lerche, Physics Of Plasmas **13** (2006).
7. M. D. Wilke, S. H. Batha, P. A. Bradley, R. D. Day, D. D. Clark, V. E. Fatherley, . . . D. C. Wilson, Review of Scientific Instruments **79**, 10E529 (5 pp.) (2008).
8. D. C. Wilson, G. P. Grim, I. L. Tregillis, M. D. Wilke, M. V. Patel, S. M. Sepke, . . . R. Buckles, Review Of Scientific Instruments **81** (2010).
9. S. C. Burkhart, E. Bliss, P. Di Nicola, D. Kalantar, R. Lowe-Webb, T. McCarville, . . . K. Wilhelmsen, Applied Optics **50**, 1136 (2011).
10. R. M. Malone, B. C. Cox, V. E. Fatherley, B. C. Frogget, G. P. Grim, M. I. Kaufman, . . . M. D. Wilke, in *Optical System Alignment, Tolerancing, and Verification Iv*, edited by J. Sasian and R. N. Youngworth (2010), Vol. 7793.
11. V. I. Gelfgat, E. L. Kosarev, and E. R. Podolyak, Computer Physics Communications **74**, 335 (1993).